

# Synthesis and Photophysical, Electrochemical, and Electrophosphorescent Properties of a Series of Iridium(III) Complexes Based on Quinoline Derivatives and Different $\beta$ -Diketonate Ligands

Qiang Zhao,<sup>†</sup> Chang-Yun Jiang,<sup>‡</sup> Mei Shi,<sup>†</sup> Fu-You Li,<sup>\*,†</sup> Tao Yi,<sup>†</sup> Yong Cao,<sup>‡</sup> and Chun-Hui Huang<sup>\*,†</sup>

Laboratory of Advanced Materials, Fudan University, Shanghai 200433, People's Republic of China, and Institute of Polymer Optoelectronic Materials and Devices, South China University of Technology, Guangzhou 510640, People's Republic of China

Received January 12, 2006

The synthesis and photophysical, electrochemical, and electrophosphorescent properties of a series of cyclometalated iridium(III) complexes based on quinoline derivatives (C $\wedge$ N) and different  $\beta$ -diketonate ligands are reported. The iridium complexes contain two quinoline derivatives (C $\wedge$ N) and a single monoanionic  $\beta$ -diketone (LX), i.e., Ir(C $\wedge$ N)<sub>2</sub>(LX), where LX denotes acetylacetonate (acac) or 1-phenyl-3-methyl-4-isobutryryl-5-pyrazolonate (PMIP). Most of the iridium complexes in solution show phosphorescent emission with high quantum efficiencies (0.05–0.25) and microsecond lifetimes (0.5–1.67  $\mu$ s). The intense phosphorescent emission of these complexes is the result of significant spin–orbit coupling of the iridium center. By modification of the chemical structures of quinoline derivative ligands, the emissive wavelengths of complexes can be tuned from 596 to 634 nm. Interestingly, the photoluminescence quantum efficiency can be improved by the replacement of acac with PMIP. Energy transfer from the hosts poly(9,9-dioctylfluorene) (PFO) and 2-(4-biphenyl)-5-(4-*tert*-butylphenyl)-1,3,4-oxadiazole (PBD) to the guest iridium complex was investigated. Moreover, three iridium complexes were used as dopants to fabricate electrophosphorescent polymer-based light-emitting diodes (PLEDs). The PLEDs show red emission with high external quantum efficiencies, ranging from 7.0 to 9.6%.

## Introduction

Highly efficient light-emitting diodes (LEDs)<sup>1</sup> having saturated red emission with Commission Internationale de L'Éclairage (CIE) chromaticity coordinates at  $x = 0.67$ ,  $y = 0.33$  have attracted greater and greater attention for their application in full-color flat-panel displays.<sup>2</sup> Previously, saturated red emission with external quantum efficiency ( $\eta_{\text{ext}}$ ) of more than 3.8 photon/electron percent (ph/el%) was reported for a fluorescent polymer.<sup>3</sup> However, according to simple spin-pairing statistics, the singlet-exciton formation probability in the charge recombination process of fluorescent LEDs is only 25%, although this ratio might be higher in conjugated polymers.<sup>4</sup> To overcome the upper limit of singlet-exciton formation, phosphorescent heavy-metal complexes have been successfully used in organic and polymer LEDs to facilitate the mixed singlet and triplet metal-to-ligand charge-transfer (MLCT) states and fully utilize

both singlet and triplet excitons, thus providing the opportunity to realize an internal quantum efficiency of close to 100%.<sup>5</sup>

At present, iridium(III) complexes<sup>6</sup> are the best phosphorescent dyes, due to their relatively short excited-state lifetime, high photoluminescence efficiency, and excellent color tuning. Some efficient red-emitting electrophosphorescent LEDs employing iridium complexes doped into a host of small molecules have been reported by Adachi, Su, and Tsuboyama, showing near-saturated red ( $x = 0.68$ ,  $y = 0.32$ ) emission with a very high  $\eta_{\text{ext}}$  value (7–10.3 ph/el%).<sup>7</sup> In the red-emitting iridium complexes, 1-phenylisoquinoline is one of the most important ligands. For example, Jiang et al. demonstrated saturated red-

\* To whom correspondence should be addressed. Fax: 86-21-55664621. Tel: 86-21-55664185. E-mail: fyli@fudan.edu.cn (F.-Y.L.); chuang@pku.edu.cn (C.-H.H.)

<sup>†</sup> Fudan University.

<sup>‡</sup> South China University of Technology.

(1) (a) Burroughes, J. H.; Bradley, D. D. C.; Brown, A. R.; Marks, R. N.; MacKay, K.; Friend, R. H.; Burn, P. L.; Holmes, A. B. *Nature* **1990**, *347*, 539. (b) Gustafsson, G.; Cao, Y.; Treacy, G. M.; Klavetter, F.; Colaneri, N.; Heeger, A. J. *Nature* **1992**, *357*, 477.

(2) Niu, Y. H.; Tung, Y. L.; Chi, Y.; Shu, C. F.; Kim, J. H.; Chen, B.; Luo, J.; Carty, A. J.; Jen, A. K. Y. *Chem. Mater.* **2005**, *17*, 3532.

(3) Niu, Y. H.; Huang, J.; Cao, Y. *Adv. Mater.* **2003**, *15*, 807.

(4) (a) Cao, Y.; Parker, I. D.; Yu, G.; Zhang, C.; Heeger, A. J. *Nature* **1999**, *397*, 414. (b) Wohlgenannt, M.; Tandon, K.; Mazumdar, S.; Ramasesha, S.; Vardeny, Z. V. *Nature* **2001**, *409*, 494.

(5) (a) Adachi, C.; Baldo, M. A.; Thompson, M. E.; Forrest, S. R. *J. Appl. Phys.* **2001**, *90*, 5048. (b) Ikai, M.; Tokito, S.; Sakamoto, Y.; Suzuki, T.; Taga, Y. *Appl. Phys. Lett.* **2001**, *79*, 156. (c) Baldo, M. A.; O'Brien, D. F.; You, Y.; Shoustikov, A.; Sibley, S.; Thompson, M. E.; Forrest, S. R. *Nature* **1998**, *395*, 151. (d) Lu, W.; Mi, B. X.; Chan, M. C. W.; Hui, Z.; Che, C. M.; Zhu, N.; Lee, S. T. *J. Am. Chem. Soc.* **2004**, *126*, 4958–4971. (e) Chan, S. C.; Chan, M. C. W.; Wang, Y.; Che, C. M.; Cheung, K. K.; Zhu, N. *Chem. Eur. J.* **2001**, *7*, 4180–4190.

(6) (a) Lamansky, S.; Djurovich, P.; Murphy, D.; Abdel-Razzaq, F.; Lee, H. E.; Adachi, C.; Burrows, P. E.; Forrest, S. R.; Thompson, M. E. *J. Am. Chem. Soc.* **2001**, *123*, 4304. (b) Zhu, W.; Mo, Y.; Yuan, M.; Yang, W.; Cao, Y. *Appl. Phys. Lett.* **2002**, *80*, 2045. (c) Gong, X.; Ostrowski, J. C.; Bazan, G. C.; Moses, D.; Heeger, A. J. *Appl. Phys. Lett.* **2002**, *81*, 3711. (d) Hwang, F. M.; Chen, H. Y.; Chen, P. S.; Liu, C. S.; Chi, Y.; Shu, C. F.; Wu, F. I.; Chou, P. T.; Peng, S. M.; Lee, G. H. *Inorg. Chem.* **2005**, *44*, 1344. (e) Li, H. C.; Chou, P. T.; Hu, Y. H.; Cheng, Y. M.; Liu, R. S. *Organometallics* **2005**, *24*, 1329. (f) Kwon, T. H.; Cho, H. S.; Kim, M. K.; Kim, J. W.; Kim, J. J.; Lee, K. H.; Park, S. J.; Shin, I. S.; Kim, H.; Shin, D. M.; Chung, Y. K.; Hong, J. I. *Organometallics* **2005**, *24*, 1578. (g) Huang, C. H.; Li, F. Y.; Huang, W. *Introduction to Organic Light-Emitting Materials and Devices*; Press of Fudan University: Shanghai, People's Republic of China, 2005.

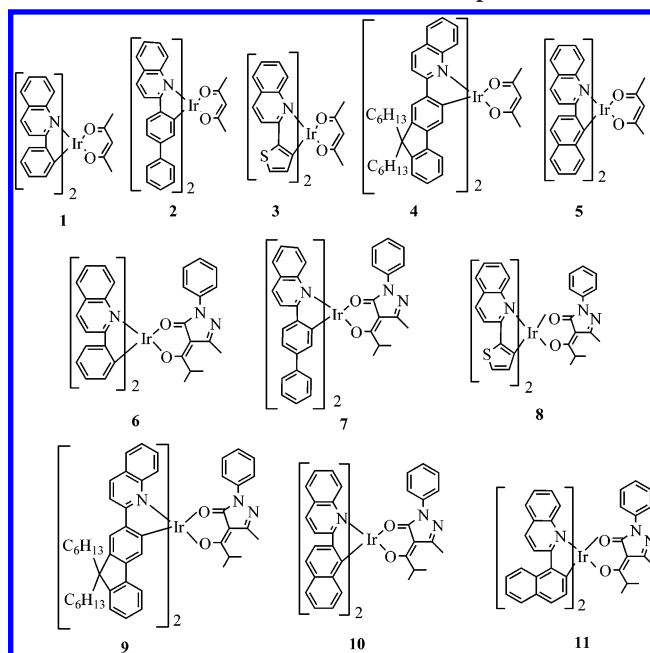
emitting ( $x = 0.67$ ,  $y = 0.33$ ) LEDs with  $\eta_{\text{ext}} = 12$  ph/eV% by doping bis(1-phenylisoquinolyl)(acetylacetonate)iridium into the blends of poly(9,9-dioctylfluorene) (PFO) and 2-(4-biphenyl)-5-(4-*tert*-butylphenyl)-1,3,4-oxadiazole (PBD).<sup>8a</sup> In addition, Neher and Meerholz achieved high-efficiency red-emitting LEDs and  $\eta_{\text{ext}}$  can reach 13%.<sup>8b</sup> Generally, the synthesis of 1-phenylisoquinoline is complicated. As an isomer of 1-phenylisoquinoline, 2-phenylquinoline is not a satisfactory ligand for red-emitting iridium complexes, because orange-red emission ( $\lambda_{\text{max}} = 597$  nm) was observed for bis(2-phenylquinolyl)(acetylacetonate)iridium.<sup>9</sup> However, 2-phenylquinoline can be easily synthesized by Friedländer condensation<sup>10</sup> in high yield, at low cost, in a short reaction time, and with facile manipulation without N<sub>2</sub> protection. Also, color tuning can be achieved by a simple modification of the ligand. Therefore, good red-emitting iridium complexes based on quinoline derivative ligands may be obtained and it is of interest to investigate this class of complexes. On the other hand, there have been few reports about the effect of different  $\beta$ -diketonate ligands on the photophysical and electroluminescent properties of the iridium complexes.<sup>6a</sup> Thompson et al.<sup>6a</sup> reported iridium complexes with several  $\beta$ -diketonate ligands (such as tmd, bza, and dbm). When the triplet-state energy levels of  $\beta$ -diketonate ligands are lower than <sup>3</sup>LC ( $\pi(\text{C}\wedge\text{N})-\pi^*(\text{C}\wedge\text{N})$ ) and <sup>3</sup>MLCT ( $d\pi(\text{Ir})-\pi^*(\text{C}\wedge\text{N})$ ), a triplet  $\beta$ -diketonate ligand level will be the lowest energy excited state and the luminescent quantum yields of the iridium complexes are reduced. Therefore, it would be interesting to investigate the influence of other  $\beta$ -diketonate ligands on the photophysical, electrochemical, and electrophosphorescent properties of iridium complexes.

Herein, we report the synthesis and characterization of a series of new iridium complexes, **1–11** (see Chart 1), based on quinoline derivatives and different  $\beta$ -diketonate ligands. By modification of the chemical structures of quinoline derivatives, the emissive color of the iridium complexes can be tuned from orange-red to saturated red. Interestingly, the photoluminescence efficiency can be improved by simply substituting acetylacetonate (acac) with another kind of  $\beta$ -diketonate ligand 1-phenyl-3-methyl-4-isobutryl-5-pyrazolonate (PMIP). Moreover, efficient electrophosphorescent polymer-based light-emitting diodes (PLEDs) were fabricated by doping the complexes **2**, **5**, and **7** into a host composed of PFO and PBD.

## Experimental Section

**Materials.** Poly(ethylenedioxythiophene)-poly(styrenesulfonic acid) (PEDOT:PSS) was purchased from Aldrich. Acetylacetone, 2-aminobenzaldehyde, 4-acetylphenyl, 2-acetylthiophene, 1-acetylnaphthalene, 2-acetylnaphthalene, and 2-acetylfluorene were obtained from Acros and used without further purification. PMIP was prepared according to the method in the literature.<sup>11</sup> 9,9-Dihexyl-2-acetylfluorene was synthesized by the reaction of 2-acetylfluorene

Chart 1. Molecular Structures of Complexes **1–11**



and 1-bromohexane in the presence of KOH and was characterized by its <sup>1</sup>H NMR spectrum.<sup>12</sup>

**General Experiments.** NMR spectra were taken on Mercury Plus 400 MHz NMR spectrometer. The elemental analyses were performed on a VarioEL III O-Element Analyzer system. Mass spectra were obtained on a Shimadzu matrix-assisted laser desorption/ionization time-of-flight mass spectrometer (MALDI-TOF-MASS). UV-visible absorption spectra were recorded using a Shimadzu 3000 UV-vis-near-IR spectrophotometer. The photoluminescence spectra were measured on an Edinburgh LFS920 fluorescence spectrophotometer. The luminescence quantum yields of the iridium complexes in solution were measured with reference to quinine sulfate ( $\Phi_{\text{F}} = 0.56$  in 1 mol L<sup>-1</sup> sulfuric acid). The solutions were degassed by three freeze-pump-thaw cycles. The photoluminescent lifetime was recorded on a single photon counting spectrometer from Edinburgh Instruments (FLS920) with a hydrogen-filled pulse lamp as the excitation source. The data were analyzed by iterative convolution of the luminescence decay profile with the instrument response function using the software package provided by Edinburgh Instruments. Measurement of the absolute photoluminescence efficiency was performed on a Labsphere IS-080 (8 in.) instrument, which contained an integrating sphere coated on the inside with barium sulfate reflecting material, and the diameter of the integrating sphere was 8 in. The excitation wavelength was 374 nm. The photoluminescence efficiency was calculated from the software provided with the Labsphere IS-080 (8 in.).

**Electrochemical Measurements.** Electrochemical measurements were carried out in a one-compartment cell, under an N<sub>2</sub> atmosphere, equipped with a glassy-carbon working electrode, a platinum-wire counter electrode, and a Ag/Ag<sup>+</sup> reference electrode with an Eco Chemie Autolab. Measurements of oxidation and reduction were undertaken in anhydrous solutions of CH<sub>2</sub>Cl<sub>2</sub> and THF, respectively, containing the supporting electrolyte 0.10 mol L<sup>-1</sup> tetrabutylammonium hexafluorophosphate (Bu<sub>4</sub>N<sup>+</sup>PF<sub>6</sub><sup>-</sup>). The scan rate was 100 mV s<sup>-1</sup>.

**Synthesis of Quinoline Derivative Ligands (L1–L6).** The quinoline derivative ligands **L1–L6** were obtained by Friedländer condensation<sup>10</sup> (as shown in Scheme 1) as follows: saturated ethanolic NaOH was added to a mixture of 2-aminobenzaldehyde (7.8 mmol) and the acetylaryl compound (7.8 mmol) in absolute

(7) (a) Adachi, C.; Baldo, M. A.; Forrest, S. R.; Lamansky, S.; Thompson, M. E.; Kwong, R. C. *Appl. Phys. Lett.* **2001**, *78*, 1622. (b) Su, Y. J.; Huang, H. L.; Li, C. L.; Chien, C. H.; Tao, Y. T.; Chou, P. T.; Satta, S.; Liu, R. S. *Adv. Mater.* **2003**, *15*, 884. (c) Tsuboyama, A.; Iwakaki, H.; Furugori, M.; Mukai, T.; Kamatani, J.; Igawa, S.; Moriyama, T.; Miura, S.; Takiguchi, T.; Okada, S.; Hoshino, M.; Ueno, K. *J. Am. Chem. Soc.* **2003**, *125*, 12971.

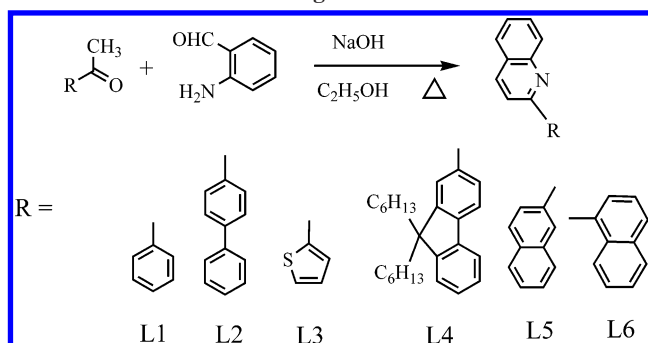
(8) (a) Jiang, C. Y.; Yang, W.; Peng, J. B.; Xiao, S.; Cao, Y. *Adv. Mater.* **2004**, *16*, 537. (b) Yang, X. H.; Müller, D. C.; Neher, D.; Meerholz, K. *Adv. Mater.* **2006**, *18*, 948.

(9) Lamansky, S.; Djurovich, P.; Murphy, D.; Abdel-Razzaq, F.; Kwong, R.; Tsyba, I.; Bortz, M.; Mui, B.; Bau, R.; Thompson, M. E. *Inorg. Chem.* **2001**, *40*, 1704.

(10) Hu, Y. Z.; Zhang, G.; Thummel, R. P. *Org. Lett.* **2003**, *5*, 2251.

(11) Shi, M.; Li, F. Y.; Yi, T.; Zhang, D. Q.; Hu, H. M.; Huang, C. H. *Inorg. Chem.* **2005**, *44*, 8929–8936.

(12) Liu, M. S.; Luo, J.; Jen, A. K. Y. *Chem. Mater.* **2003**, *15*, 3496.

**Scheme 1. Synthetic Route and Molecular Structures of the Ligands**

ethanol, and the mixture was refluxed overnight. After the mixture was cooled, the precipitate was collected by filtration and recrystallized from  $\text{CH}_2\text{Cl}_2$  solution to obtain the corresponding ligand.

**L1.**<sup>6b</sup> White crystal. Yield: 80%.  $^1\text{H NMR}$  (400 MHz,  $\text{CDCl}_3$ , 298 K;  $\delta$  (ppm)): 8.23 (d,  $J = 8.4$  Hz, 1H), 8.18 (m, 3H), 7.89 (d,  $J = 8.4$  Hz, 1H), 7.84 (d,  $J = 8.0$  Hz, 1H), 7.73 (t,  $J = 7.2$  Hz, 1H), 7.54 (t,  $J = 8.0$  Hz, 3H), 7.47 (t,  $J = 7.2$  Hz, 1H). Anal. Calcd for  $\text{C}_{15}\text{H}_{11}\text{N}$ : C, 87.77; H, 5.40; N, 6.82. Found: C, 87.50; H, 5.55; N, 6.63.

**L2.**<sup>13</sup> White crystal. Yield: 78%.  $^1\text{H NMR}$  (400 MHz,  $\text{CDCl}_3$ , 298 K;  $\delta$  (ppm)): 8.19–8.28 (m, 4H), 7.93 (d,  $J = 8.4$  Hz, 1H), 7.84 (d,  $J = 8.0$  Hz, 1H), 7.73–7.79 (m, 3H), 7.68 (d,  $J = 7.2$  Hz, 2H), 7.46–7.56 (m, 3H), 7.39 (m, 1H). Anal. Calcd for  $\text{C}_{21}\text{H}_{15}\text{N}$ : C, 89.65; H, 5.37; N, 4.98. Found: C, 89.52; H, 5.12; N, 4.77.

**L3.** White sheet crystal. Yield: 70%.  $^1\text{H NMR}$  (400 MHz,  $\text{CDCl}_3$ , 298 K;  $\delta$  (ppm)): 8.11 (m, 2H), 7.67–7.81 (m, 4H), 7.48 (m, 2H), 7.16 (t,  $J = 5.2$  Hz, 1H). Anal. Calcd for  $\text{C}_{13}\text{H}_9\text{NS}$ : C, 73.90; H, 4.29; N, 6.63. Found: C, 73.74; H, 4.42; N, 6.43.

**L4.** White crystal. Yield: 68%.  $^1\text{H NMR}$  (400 MHz,  $\text{CDCl}_3$ , 298 K;  $\delta$  (ppm)): 8.11–8.19 (m, 3H), 8.06 (s, 1H), 7.88 (d,  $J = 8.4$  Hz, 1H), 7.77 (d,  $J = 7.6$  Hz, 2H), 7.69 (m, 2H), 7.46 (t,  $J = 7.2$  Hz, 1H), 7.24–7.32 (m, 3H), 1.99 (m, 4H), 0.90–1.05 (m, 12H), 0.53–0.69 (m, 10H). Anal. Calcd for  $\text{C}_{34}\text{H}_{39}\text{N}$ : C, 88.45; H, 8.51; N, 3.03. Found: C, 88.23; H, 8.63; N, 2.87.

**L5.** White crystal. Yield: 71%.  $^1\text{H NMR}$  (400 MHz,  $\text{CDCl}_3$ , 298 K;  $\delta$  (ppm)): 8.63 (s, 1H), 8.38 (d,  $J = 6.8$  Hz, 1H), 8.27 (m, 2H), 7.99–8.07 (m, 3H), 7.85–7.92 (m, 2H), 7.76 (t,  $J = 7.6$  Hz, 1H), 7.55 (m, 3H). Anal. Calcd for  $\text{C}_{19}\text{H}_{13}\text{N}$ : C, 89.38; H, 5.13; N, 5.49. Found: C, 89.21; H, 5.01; N, 5.37.

**L6.** Oily liquid. Yield: 70%.  $^1\text{H NMR}$  (400 MHz,  $\text{CDCl}_3$ , 298 K;  $\delta$  (ppm)): 8.25–8.30 (t,  $J = 8.8$  Hz, 2H), 8.19 (d,  $J = 8.0$  Hz, 1H), 7.95–7.98 (t,  $J = 7.2$  Hz, 2H), 7.89 (m, 1H), 7.75–7.82 (m, 2H), 7.72 (d,  $J = 8.0$  Hz, 1H), 7.59–7.64 (m, 2H), 7.49–7.54 (m, 2H). Anal. Calcd for  $\text{C}_{19}\text{H}_{13}\text{N}$ : C, 89.38; H, 5.13; N, 5.49. Found: C, 89.72; H, 5.45; N, 5.21.

**Synthesis of Iridium Complexes 1–11.** Complex **1** was synthesized according to a method given previously in the literature.<sup>9</sup> A mixture of 2-ethoxyethanol and water (3:1, v/v) was added to a flask containing  $\text{IrCl}_3 \cdot 3\text{H}_2\text{O}$  (1 mmol) and L1 (2.5 mmol). The mixture was refluxed for 24 h. After the mixture was cooled, the red solid precipitate was filtered to give the crude cyclometalated Ir(III) chloro-bridged dimer. To the mixture of crude chloro-bridged dimer (0.2 mmol) and  $\text{Na}_2\text{CO}_3$  (1.4 mmol) were added 2-ethoxyethanol and acetylacetonate (0.5 mmol), and then the slurry was refluxed for 12 h. After the mixture was cooled to room temperature, the red precipitate was collected by filtration and was chromatographed using  $\text{CH}_2\text{Cl}_2$ /petroleum ether (2:1, v/v) to give complex **1**. The other cyclometalated Ir(III) complexes **2–11** were prepared by a procedure similar to that for **1**. The iridium complexes were characterized by  $^1\text{H NMR}$ , elemental analysis, and

MALDI-TOF-MASS spectrometry. Moreover, **2** and **3** were further identified by single-crystal X-ray analysis.

**Complex 2.** Red powder. Yield: 43%.  $^1\text{H NMR}$  (400 MHz,  $\text{CDCl}_3$ , 298 K;  $\delta$  (ppm)): 8.58 (d,  $J = 7.6$  Hz, 2H), 8.18 (d, 2H), 8.08 (d,  $J = 8.4$  Hz, 2H), 7.86 (d,  $J = 8.0$  Hz, 2H), 7.80–7.85 (m, 2H), 7.45–7.53 (m, 4H), 7.07–7.17 (m, 12H), 6.75 (s, 2H), 4.68 (s, 1H), 1.53 (s, 6H). Anal. Calcd for  $\text{IrC}_{47}\text{H}_{35}\text{N}_2\text{O}_2$ : C, 66.26; H, 4.14; N, 3.29. Found: C, 66.01; H, 3.97; N, 2.95. MS (LDI-TOF;  $m/e$ ): 852.

**Complex 3.** Red powder. Yield: 40%.  $^1\text{H NMR}$  (400 MHz,  $\text{CDCl}_3$ , 298 K;  $\delta$  (ppm)): 8.36 (d,  $J = 7.2$  Hz, 2H), 8.04 (d,  $J = 8.4$  Hz, 2H), 7.70–7.76 (m, 4H), 7.41–7.47 (m, 4H), 7.12 (d,  $J = 4.8$  Hz, 2H), 6.25 (d,  $J = 4.8$  Hz, 2H), 4.83 (s, 1H), 1.62 (s, 6H). Anal. Calcd for  $\text{IrC}_{31}\text{H}_{23}\text{N}_2\text{O}_2\text{S}_2$ : C, 52.30; H, 3.26; N, 3.94. Found: C, 52.01; H, 2.99; N, 3.63. MS (LDI-TOF;  $m/e$ ): 712.

**Complex 4.** Red powder. Yield: 37%.  $^1\text{H NMR}$  (400 MHz,  $\text{CDCl}_3$ , 298 K;  $\delta$  (ppm)): 8.48 (d,  $J = 8.4$  Hz, 2H), 8.18–8.25 (m, 4H), 7.76–7.82 (m, 4H), 7.43 (t,  $J = 6.8$  Hz, 2H), 7.37 (t,  $J = 7.2$  Hz, 2H), 7.21 (d,  $J = 7.6$  Hz, 2H), 7.10 (t,  $J = 7.6$  Hz, 2H), 6.98–7.05 (m, 4H), 6.86 (s, 2H), 4.68 (s, 1H), 1.90–1.98 (m, 8H), 1.51 (s, 6H), 1.11–1.20 (m, 16H), 0.60–0.99 (m, 28H). Anal. Calcd for  $\text{IrC}_{73}\text{H}_{83}\text{N}_2\text{O}_2$ : C, 72.30; H, 6.90; N, 2.31. Found: C, 72.14; H, 7.11; N, 2.54. MS (LDI-TOF;  $m/e$ ): 1212.

**Complex 5.** Red powder. Yield: 36%.  $^1\text{H NMR}$  (400 MHz,  $\text{CDCl}_3$ , 298 K;  $\delta$  (ppm)): 8.65 (d,  $J = 8.0$  Hz, 1H), 8.57 (d,  $J = 8.4$  Hz, 2H), 8.27–8.37 (m, 6H), 7.85 (d,  $J = 8.0$  Hz, 2H), 7.76 (d,  $J = 7.6$  Hz, 2H), 7.48 (t,  $J = 7.6$  Hz, 2H), 7.40 (t,  $J = 6.8$  Hz, 2H), 7.05–7.10 (m, 5H), 6.89 (s, 2H), 4.61 (s, 1H), 1.45 (s, 6H). Anal. Calcd for  $\text{IrC}_{43}\text{H}_{31}\text{N}_2\text{O}_2$ : C, 64.56; H, 3.91; N, 3.50. Found: C, 64.25; H, 3.74; N, 3.39. MS (LDI-TOF;  $m/e$ ): 800.

**Complex 6.** Pink powder. Yield: 50%.  $^1\text{H NMR}$  (400 MHz,  $\text{CDCl}_3$ , 298 K;  $\delta$  (ppm)): 8.48 (d,  $J = 8.4$  Hz, 1H), 8.24 (d,  $J = 8.8$  Hz, 1H), 8.04–8.18 (m, 4H), 7.83–7.89 (m, 2H), 7.75 (d,  $J = 8.0$  Hz, 1H), 7.68 (d,  $J = 8.0$  Hz, 3H), 7.42 (t,  $J = 7.2$  Hz, 1H), 7.28–7.36 (m, 2H), 7.18 (t,  $J = 7.6$  Hz, 2H), 6.96–7.04 (m, 4H), 6.56–6.66 (m, 4H), 2.77–2.84 (m, 1H), 2.03 (s, 3H), 0.96 (d,  $J = 6.4$  Hz, 3H), 0.35 (d,  $J = 6.8$  Hz, 3H). Anal. Calcd for  $\text{IrC}_{44}\text{H}_{35}\text{N}_4\text{O}_2$ : C, 62.62; H, 4.18; N, 6.64. Found: C, 62.43; H, 4.42; N, 6.39. MS (LDI-TOF;  $m/e$ ): 844.

**Complex 7.** Pink powder. Yield: 43%.  $^1\text{H NMR}$  (400 MHz,  $\text{CDCl}_3$ , 298 K;  $\delta$  (ppm)): 8.15 (d,  $J = 8.4$  Hz, 1H), 8.01 (d,  $J = 8.2$  Hz, 1H), 7.64–7.78 (m, 4H), 7.45–7.54 (m, 2H), 7.37 (d,  $J = 8.4$  Hz, 1H), 7.31 (d,  $J = 8.4$  Hz, 3H), 7.04 (t,  $J = 8.0$  Hz, 1H), 6.90–6.99 (m, 2H), 6.80–6.85 (m, 4H), 6.65–6.74 (m, 10H), 6.58–6.64 (t,  $J = 8.0$  Hz, 2H), 6.40 (d,  $J = 8.0$  Hz, 2H), 2.70–2.83 (m, 1H), 1.99 (s, 3H), 0.96 (d,  $J = 6.4$  Hz, 3H), 0.39 (d,  $J = 6.8$  Hz, 3H). Anal. Calcd for  $\text{IrC}_{56}\text{H}_{43}\text{N}_4\text{O}_2$ : C, 67.52; H, 4.35; N, 5.62. Found: C, 67.31; H, 4.22; N, 5.86. MS (LDI-TOF;  $m/e$ ): 996.

**Complex 8.** Red powder. Yield: 43%.  $^1\text{H NMR}$  (400 MHz,  $\text{CDCl}_3$ , 298 K;  $\delta$  (ppm)): 8.36 (d,  $J = 8.8$  Hz, 1H), 8.11 (d,  $J = 8.8$  Hz, 1H), 7.99–8.05 (m, 2H), 7.74–7.76 (m, 3H), 7.67–7.70 (m, 2H), 7.62 (d,  $J = 8.0$  Hz, 1H), 7.35–7.38 (m, 2H), 7.24–7.26 (m, 3H), 7.17–7.19 (t,  $J = 4.8$  Hz, 2H), 7.04–7.08 (t,  $J = 7.2$  Hz, 1H), 6.97–7.01 (t,  $J = 7.2$  Hz, 1H), 6.36 (d,  $J = 4.8$  Hz, 2H), 2.86–2.93 (m, 1H), 2.10 (s, 3H), 1.03 (d,  $J = 6.4$  Hz, 3H), 0.46 (d,  $J = 6.8$  Hz, 3H). Anal. Calcd for  $\text{IrC}_{40}\text{H}_{31}\text{N}_4\text{O}_2\text{S}_2$ : C, 56.12; H, 3.65; N, 6.54. Found: C, 56.63; H, 3.17; N, 6.75. MS (LDI-TOF;  $m/e$ ): 856.

**Complex 9.** Red powder. Yield: 35%.  $^1\text{H NMR}$  (400 MHz,  $\text{CDCl}_3$ , 298 K;  $\delta$  (ppm)): 8.42 (d,  $J = 8.8$  Hz, 1H), 8.17–8.24 (m, 5H), 7.90 (s, 1H), 7.79–7.83 (t,  $J = 7.6$  Hz, 3H), 7.75 (d,  $J = 7.2$  Hz, 1H), 7.67 (d,  $J = 7.2$  Hz, 1H), 7.34–7.37 (t,  $J = 7.6$  Hz, 1H), 6.98–7.24 (m, 15H), 6.77–6.82 (t,  $J = 7.2$  Hz, 1H), 2.76–2.82 (m, 1H), 1.95–2.02 (m, 7H), 1.03–1.26 (m, 23H), 0.60–0.88 (m, 28H), 0.42 (d,  $J = 6.8$  Hz, 3H). Anal. Calcd for  $\text{IrC}_{82}\text{H}_{91}\text{N}_4\text{O}_2$ : C, 72.59; H, 6.76; N, 4.13. Found: C, 72.65; H, 6.16; N, 4.72. MS (LDI-TOF;  $m/e$ ): 1357.

(13) (a) Thummel, R. P.; Lefoulon, F.; Cantu, D.; Mahadevan, R. *J. Org. Chem.* **1984**, *49*, 2208. (b) Caluwe, P. *Tetrahedron* **1980**, *36*, 2359.

**Complex 10.** Red powder. Yield: 35%.  $^1\text{H}$  NMR (400 MHz,  $\text{CDCl}_3$ , 298 K;  $\delta$  (ppm)): 8.58 (d,  $J = 8.8$  Hz, 1H), 8.26–8.44 (m, 7H), 7.79–7.85 (m, 3H), 7.75 (d,  $J = 8.0$  Hz, 1H), 7.64 (d,  $J = 8.0$  Hz, 2H), 7.42–7.46 (t,  $J = 7.6$  Hz, 1H), 7.29–7.34 (m, 2H), 7.12–7.20 (m, 8H), 6.99 (m, 3H), 6.91 (s, 1H), 2.76–2.82 (m, 1H), 2.02 (s, 3H), 0.90 (d,  $J = 6.8$  Hz, 3H), 0.36 (d,  $J = 6.8$  Hz, 3H). Anal. Calcd for  $\text{IrC}_{52}\text{H}_{39}\text{N}_4\text{O}_2$ : C, 66.15; H, 4.16; N, 5.93. Found: C, 66.39; H, 4.55; N, 5.68. MS (LDI-TOF;  $m/e$ ): 944.

**Complex 11.** Red powder. Yield: 41%.  $^1\text{H}$  NMR (400 MHz,  $\text{CDCl}_3$ , 298 K;  $\delta$  (ppm)): 8.68–8.79 (m, 4H), 8.17–8.25 (m, 3H), 8.11 (d,  $J = 9.2$  Hz, 1H), 7.43–7.79 (m, 7H), 7.35–7.44 (m, 3H), 7.28 (t,  $J = 8.4$  Hz, 3H), 6.48–7.15 (m, 6H), 6.69 (d,  $J = 8.0$  Hz, 1H), 6.63 (d,  $J = 8.0$  Hz, 1H), 2.78–2.87 (m, 1H), 2.05 (s, 3H), 0.93 (d,  $J = 6.8$  Hz, 3H), 0.44 (d,  $J = 6.8$  Hz, 3H). Anal. Calcd for  $\text{IrC}_{52}\text{H}_{39}\text{N}_4\text{O}_2$ : C, 66.15; H, 4.16; N, 5.93. Found: C, 66.56; H, 4.59; N, 5.73. MS (LDI-TOF;  $m/e$ ): 944.

**Synthesis of the Gadolinium Complex  $\text{Gd}(\text{acac})_3(\text{H}_2\text{O})_2$ .**  $\text{Gd}(\text{acac})_3(\text{H}_2\text{O})_2$  was synthesized according to the method reported previously.<sup>11</sup> Anal. Calcd for  $\text{GdC}_{15}\text{H}_{25}\text{O}_8$ : C, 36.72; H, 5.14. Found: C, 36.56; H, 4.89.

**X-ray Crystallography Analysis.** The single crystals of **2** and **3** were mounted on glass fiber and transferred to a Bruker SMART CCD area detector. Crystallographic measurements were carried out using a Bruker SMART CCD diffractometer with  $\sigma$  scans and graphite-monochromated Mo  $K\alpha$  radiation ( $\lambda = 0.71073 \text{ \AA}$ ) at room temperature. The crystal structures were solved by direct methods and refined by full-matrix least squares on  $F^2$  values using the program SHELXS-97.<sup>14</sup> All non-hydrogen atoms were refined anisotropically. Hydrogen atoms were calculated in ideal geometries. For the full-matrix least-squares refinements ( $I > 2\sigma(I)$ ), the unweighted and weighted agreement factors of  $R1 = \sum(F_o - F_c)/\sum F_o$  and  $wR2 = [\sum w(F_o^2 - F_c^2)^2/\sum wF_o^4]^{1/2}$  were used. CCDC reference numbers are 282740 and 294372 for **2** and **3**, respectively.

**Fabrication and Characterization of PLED Devices.** Indium tin oxide (ITO) glass substrate with a sheet resistance of 15  $\Omega/\text{XXXXX}$  was kindly supplied by China Southern Glass Holding Co. Ltd. The fabrication of electrophosphorescent devices followed a standard procedure. A 70 nm thick layer of PEDOT:PSS was spin-cast onto precleaned ITO glass substrates. A thin layer of Ba (4 nm thickness) with an Al capping layer of 200 nm thickness was deposited through a shadow mask in a chamber with a base pressure of  $\sim 10^{-4}$  Pa. Device fabrication was carried out in a controlled-atmosphere drybox (Vacuum Atmospheres Co.) under  $\text{N}_2$  circulation. Current density ( $I$ )–voltage ( $V$ )–luminance ( $L$ ) data were collected using a Keithley 236 source measurement unit and a calibrated silicon photodiode. External electroluminescence (EL) quantum efficiencies were obtained by measuring the total light output in all directions in an integrating sphere (IS-080, Labsphere). The luminance ( $\text{cd m}^{-2}$ ) and luminous efficiency ( $\text{cd A}^{-1}$ ) were measured by a silicon photodiode and calibrated using a PR-705 SpectraScan spectrophotometer (Photo Research).

## Results and Discussion

**Synthesis of Materials.** The aryl-substituted quinoline derivatives **L1–L6** were obtained in good yield by the Friedländer condensation reaction of 2-aminobenzaldehyde with the corresponding acetylaryl compounds according to a previous procedure.<sup>10</sup> In our case, the synthetic method of iridium complexes involves two steps. First, the cyclometalated iridium chloro-bridged dimer was synthesized by the same methods reported by Nonoyama,<sup>15</sup> and then the iridium complexes were prepared by the reaction of the dimer with the corresponding  $\beta$ -diketonate ligand (acac or PMIP) in the presence of sodium carbonate. We

**Table 1. Crystallographic Data for **2** and **3****

	<b>2</b>	<b>3</b>
empirical formula	$\text{C}_{47}\text{H}_{35}\text{IrN}_2\text{O}_2$	$\text{C}_{64}\text{H}_{48}\text{Cl}_4\text{Ir}_2\text{N}_4\text{O}_4\text{S}_4$
cryst syst	monoclinic	triclinic
space group	$P2_1/c$	$P\bar{1}$
cryst size, mm	$0.40 \times 0.40 \times 0.30$	$0.20 \times 0.15 \times 0.12$
$a$ , $\text{\AA}$	14.720(4)	13.9461(10)
$b$ , $\text{\AA}$	19.528(5)	15.9730(12)
$c$ , $\text{\AA}$	13.172(3)	16.2461(16)
$\alpha$ , deg	90	71.238(15)
$\beta$ , deg	109.675(3)	77.455(15)
$\gamma$ , deg	90	67.386(15)
$V$ , $\text{\AA}^3$	3565.2(15)	3145.1(5)
$Z$	4	2
calcd density, $\text{g cm}^{-3}$	1.587	1.681
$\mu$ , $\text{mm}^{-1}$	3.788	4.579
$F(000)$	1696	1556
final R1 ( $I > 2\sigma(I)$ )	0.0276	0.0427
wR2 ( $I > 2\sigma(I)$ )	0.0622	0.1042
R1 (all data)	0.0421	0.0697
wR2 (all data)	0.0680	0.1208
GOF on $F^2$	1.025	1.010

also tried to synthesize the complex  $\text{Ir}(\text{L6})_2(\text{acac})$ . Unfortunately, this complex is difficult to purify, due to its poor solubility.

**Crystal Structures of Iridium Complexes **2** and **3**.** Single crystals of **2** and **3** were obtained from a mixed solution of  $\text{CH}_2\text{Cl}_2$  and hexane. The crystal data and details of the structure determinations are summarized in Table 1. The ORTEP diagrams of **2** and **3** are depicted in Figure 1. Some relevant bond parameters are listed in Table 2.

The iridium centers of **2** and **3** adopt a distorted-octahedral coordination geometry with cis-O,O, cis-C,C, and trans-N,N chelate disposition. All bond lengths and angles of **2** and **3** are within the normal ranges. Moreover, the Ir–C bond lengths of **2** and **3** are found to be shorter than the Ir–N bond lengths. For **2**, the biphenyl fragment of the cyclometalated ligand is not coplanar (twist angles are 40.6 and 32.2° for the two cyclometalated ligands, respectively). The difference in twist angles for the two cyclometalated ligands may be caused by steric effects. In comparison with bis(2-phenylpyridine)(acetylacetonate)iridium ( $\text{Ir}(\text{ppy})_2(\text{acac})$ ), reported previously,<sup>9</sup> **2** and **3** possess longer Ir–N bonds and narrower bite angles for the diketonate ligand chelate. The longer Ir–N bonds for **2** and **3** are due to the weaker basicity of quinoline compared with that of pyridine. Also, the bulkier quinoline derivative ligands may result in narrower bite angles.

**Photophysical Properties.** The photophysical properties of **1–11** in  $\text{CH}_2\text{Cl}_2$  solution were investigated, and the data are given in Table 3. The UV–vis absorption spectra of all complexes are shown in Figure 2. All complexes display intense absorption bands in the ultraviolet region of 280–400 nm with extinction coefficients ( $\epsilon$ ) of  $\sim 10^5$ , which are assigned to the spin-allowed  $^1\text{LC}$  transitions. The weak bands at 400–500 nm are assigned to spin-allowed  $^1\text{MLCT}$  transitions. In addition, all complexes show weaker absorption tails above 500 nm, which are attributed to spin-forbidden  $^3\text{MLCT}$  and  $^3\text{LC}$  transitions. Interestingly, a red shift of the absorption band (see Table 3) was observed for both the acac-based iridium complexes **1–5** and the PMIP-based iridium complexes **6–11**, which is probably due to an increase of effective conjugation lengths of the  $\text{C}\wedge\text{N}$  ligands from **L1** to **L6**.

The photoluminescence spectra of **1–11** are shown in Figure 3. It can be seen that all complexes emit intense luminescence at room temperature in  $\text{CH}_2\text{Cl}_2$  solution, with  $\lambda_{\text{em}}$  values ranging from 596 to 634 nm (see Table 3). A red shift of the emissive wavelength was observed for both the acac-based iridium complexes **1–5** and the PMIP-based iridium complexes **6–11**

(14) Sheldrick, G. M. *SHELXTL-Plus V5.1 Software Reference Manual*; Bruker AXS: Madison, WI, 1997.

(15) Nonoyama, K. *Bull. Chem. Soc. Jpn.* **1974**, *47*, 467.

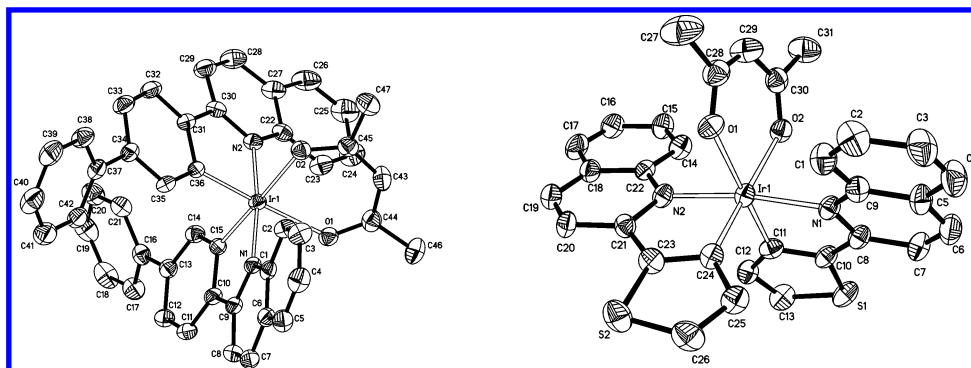


Figure 1. ORTEP diagrams of **2** and **3** with thermal ellipsoids drawn at the 30% probability level and H atoms removed for clarity.

Table 2. Selected Bond Parameters of **2**, **3**, and Ir(ppy)<sub>2</sub>(acac)

complex	Ir–C (Å)	Ir–O (Å)	Ir–N (Å)	N–Ir–N (deg)	C–Ir–C (deg)	O–Ir–O (deg)	C–Ir–N (deg)	N–Ir–O (deg)	C–Ir–O (deg)
<b>2</b>	1.981(3)	2.147(3)	2.082(3)	172.4(11)	92.5(13)	85.9(10)	95.5 (1)	104.0(1)	175.6(1)
	1.984(3)	2.164(2)	2.086(3)				93.2(12)	103.4(1)	172.0(1)
							80.2(13)	82.6(1)	87.9(1)
<b>3</b>	1.967(7)	2.151(5)	2.089(6)	171.8(2)	94.1(3)	86.4(2)	80.8(13)	80.9(1)	93.9(1)
	1.990(7)	2.161(5)	2.089(6)				93.4(3)	102.8(2)	175.3(3)
							95.1(3)	103.2(2)	174.2(3)
Ir(ppy) <sub>2</sub> (acac) <sup>9</sup>	2.003(9)	2.146(6)	2.010(9)	176.3(4)	95.2(5)	90.0(3)	80.1(3)	83.9(2)	89.3(3)
							80.2(3)	82.1(2)	90.4(3)
							95.8(4)	94.5(3)	175.6(3)
						81.7(4)	88.1(3)	87.5(3)	

Table 3. Photophysical and Electrochemical Properties of the Iridium Complexes

	$\lambda_{\text{abs}}$ , nm (log $\epsilon$ )	$\lambda_{\text{em}}$ , <sup>a</sup> nm	$\tau$ , <sup>a</sup> $\mu\text{s}$	$\Phi_{\text{em}}$ <sup>a</sup>	$E_{\text{ox}}$ , <sup>b</sup> V	$E_{\text{re}}$ , <sup>c</sup> V	$E_{\text{onset}}^{\text{ox}}$ , V	$E_{\text{onset}}^{\text{re}}$ , V	HOMO, eV	LUMO, eV	$\Delta E$ , eV
<b>1</b>	287 (5.89), 341 (5.27), 470 (4.61), 511 (4.49), 547 (4.18)	600	1.42	0.13	0.64	−2.52, −2.93	0.48	−2.21	−5.28	−2.59	2.69
<b>2</b>	287 (5.72), 354 (5.48), 408 (5.08), 473 (4.41), 558 (3.95)	605	1.53	0.19	0.58	−2.44, −2.90	0.48	−2.20	−5.28	−2.60	2.68
<b>3</b>	293 (5.57), 357 (5.37), 472 (4.83), 512 (4.81), 576 (3.78)	621	0.50, 0.94 <sup>d</sup>	0.14	0.53	−2.40, −2.91	0.45	−2.15	−5.25	−2.65	2.60
<b>4</b>	300 (5.95), 319 (5.77), 365 (5.70), 486 (4.76), 532 (4.64), 599 (3.85)	626	0.75, 0.69 <sup>d</sup>	0.11	0.45	−2.41, −2.70	0.36	−2.22	−5.16	−2.58	2.58
<b>5</b>	302 (5.84), 357 (5.53), 537 (4.23), 600 (3.01)	630	1.29	0.05	0.48	−2.30, −2.60	0.38	−2.14	−5.18	−2.66	2.52
<b>6</b>	271 (4.88), 341 (4.35), 425 (3.69), 467 (3.67), 515 (3.45), 553 (3.15)	596	0.68	0.21	0.66	−2.54, −2.95	0.49	−2.22	−5.29	−2.58	2.71
<b>7</b>	288 (4.87), 353 (4.60), 472 (3.76), 517 (3.56), 563 (3.04)	601	1.23	0.24	0.61	−2.43, −2.91	0.48	−2.21	−5.28	−2.59	2.69
<b>8</b>	287 (4.65), 351 (4.31), 418 (3.99), 507 (3.65), 575 (2.77)	620	0.98	0.25	0.55	−2.40, −3.00	0.47	−2.16	−5.27	−2.64	2.63
<b>9</b>	284 (4.80), 311 (4.76), 369 (4.71), 485 (3.87), 580 (3.15)	620	0.63, 0.76 <sup>d</sup>	0.13	0.52	−2.42, −2.81	0.47	−2.16	−5.27	−2.64	2.63
<b>10</b>	262 (4.95), 306 (4.84), 360 (4.61), 433 (3.70), 513 (3.38), 583 (2.91)	622	1.39, 0.81 <sup>d</sup>	0.11	0.51	−2.25, −2.60	0.41	−2.19	−5.21	−2.61	2.60
<b>11</b>	261 (4.78), 311 (4.48), 3.74 (4.26), 439 (3.84), 534 (3.51), 595 (2.85)	634	1.67, 0.95 <sup>d</sup>	0.10	0.48	−2.39, −2.86	0.41	−2.09	−5.21	−2.71	2.50

<sup>a</sup> Measured in CHB<sub>2</sub>ClB<sub>2</sub> solution at a concentration of  $1 \times 10^{-5}$  mol L<sup>−1</sup>. The excitation wavelength was 360 nm for all complexes. <sup>b</sup> Measured in CHB<sub>2</sub>ClB<sub>2</sub> solution. <sup>c</sup> Measured in THF solution. The scan rate was 100 mV s<sup>−1</sup>. <sup>d</sup> Measured by monitoring the shoulder band.

(see Table 3), which could be assigned to the different  $\pi$ -conjugation lengths of the C $\wedge$ N cyclometalated ligands **L1**–**L6**, indicating that the chemical structure of the C $\wedge$ N ligand correlates with the properties of iridium complexes. In addition, the difference in  $\beta$ -diketonate ligands (acac and PMIP) hardly influences the emissive wavelength of complexes with the same C $\wedge$ N ligands. However, when the acac-based iridium complexes are compared with the corresponding PMIP-based complexes with the same C $\wedge$ N ligands, it is readily found that the replacement of acac by PMIP improves the photoluminescent quantum efficiencies of the iridium complexes significantly. This improvement is very important for the design of light-emitting materials. The photoluminescence spectra of complexes **1**, **2**, and **5**–**8** are broad and featureless, indicating that the emission

originates primarily from the <sup>3</sup>MLCT state. With regard to the luminescence of complexes **3**, **4**, and **9**–**11**, a shoulder band on the lower energy side can be observed in addition to the main band, and the emission lifetimes and excitation spectra of each complex when the emissions are monitored at various energies are similar (see Table 3 and Figure S1 in the Supporting Information), which indicate that the emission of the main band and shoulder band may have the same origin from the <sup>3</sup>MLCT state.

We also compared the triplet energy level of acac with that of PMIP.<sup>11</sup> The triplet energy level of acac can be estimated by referring to the lower wavelength emission edge of the phosphorescence spectrum (see Figure S2 in the Supporting Information) of Gd(acac)<sub>3</sub>(H<sub>2</sub>O)<sub>2</sub>. Two kinds of  $\beta$ -diketonate

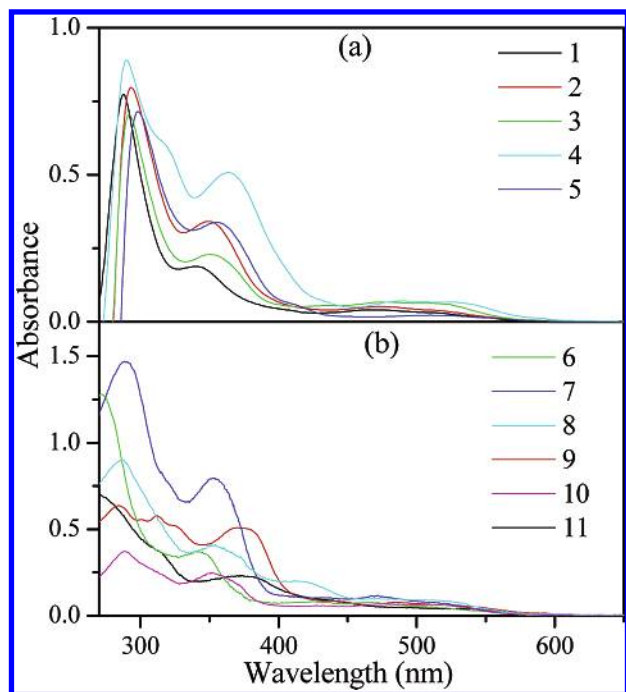


**Figure 2.** Absorption spectra of **1–5** (a) and **6–11** (b) in  $\text{CHB}_2\text{-CIB}_2$  solution at a concentration of  $1 \times 10^{-5} \text{ mol L}^{-1}$  at 298 K.

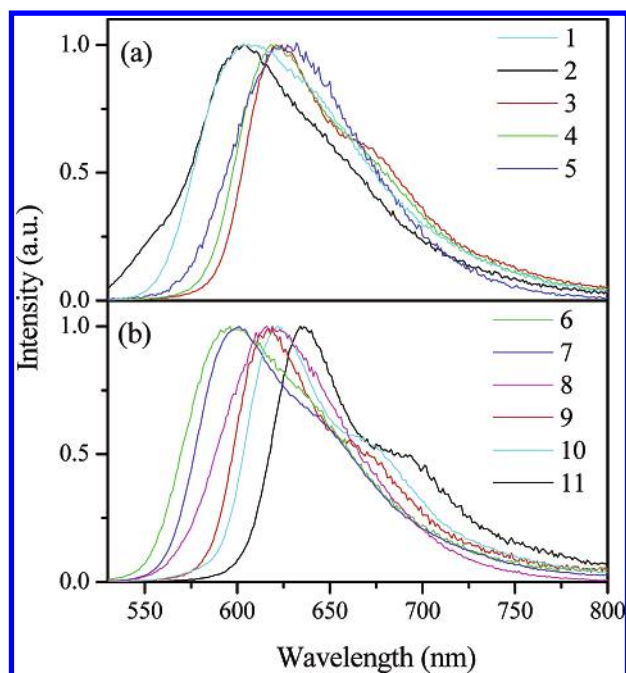


**Figure 3.** Photoluminescence spectra of **1–5** (a) and **6–11** (b) in  $\text{CHB}_2\text{-CIB}_2$  solution at a concentration of  $1 \times 10^{-5} \text{ mol L}^{-1}$  at 298 K.

ligands have similar triplet energy levels, which are 22 200 and 23 000  $\text{cm}^{-1}$  for acac and PMIP,<sup>16</sup> respectively. The relatively higher triplet level of PMIP as compared to that of acac ensures that the emission is dominated by  $^3\text{MLCT}$  ( $d\pi(\text{Ir})-\pi^*(\text{C}\backslash\text{N})$ ) transitions, leading to efficient phosphorescence.

The emission lifetimes of the emitting species, measured at 298 K in degassed solution, are in the range of 0.50–1.67  $\mu\text{s}$  (see Table 3), consistent with the previous report.<sup>6a</sup> Such long-lived excited states and their sensitivity toward oxygen indicate that the emitting states of these iridium complexes have triplet character.

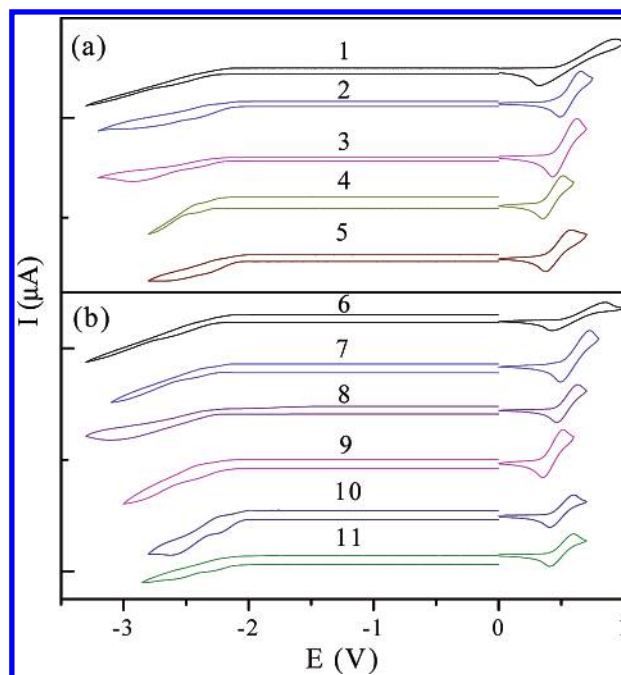


**Figure 4.** Cyclic voltammograms of **1–5** (a) and **6–11** (b).

**Electrochemical Properties.** The electrochemical properties of **1–11** in  $\text{CH}_2\text{Cl}_2$  and THF solution were studied and summarized in Table 3. All complexes show reversible oxidation waves (see Figure 4) in the range of 0.45–0.66 V versus ferrocene/ferrocenium. According to the previous electrochemical studies on iridium complexes, the oxidation process is assigned to both the Ir center and the cyclometalated ligands.<sup>6d,17,18</sup> In addition, all complexes exhibit two reduction processes. The HOMO and LUMO levels of all complexes were calculated according to the equation  $\text{HOMO/LUMO (eV)} = -(4.8 + E_{\text{onset}})$ .<sup>18</sup> Also, the energy gap between the HOMO and LUMO can be deduced by the equation  $\Delta E = \text{LUMO} - \text{HOMO}$ . It can be seen from Table 3 that the energy gap  $\Delta E$  becomes lower for both the acac-based iridium complexes **1–5** and the PMIP-based iridium complexes **6–11**, which is in accordance with the red shift of the emissive wavelength. For complexes with the same  $\text{C}\backslash\text{N}$  cyclometalated ligands, the complexes containing PMIP display higher oxidation potentials than those containing acac do.

**Energy Transfer from the Host to the Guest.** It is well-known that the dominant mechanism in the polymer–organometallic emitter system are Förster energy transfer and/or charge trapping.<sup>19</sup> Herein, as the guest, **2** was doped into the host PFO–PBD (30 wt %), and the energy transfer from the host to the guest was studied. A suitable overlap between the emission of the host PFO–PBD (30 wt %) and the absorption of **2** can be observed (see Figure S3 in the Supporting Information), which ensures an efficient Förster energy transfer from the host to the guest.

To investigate the influence of the doping concentration of the guest on the photophysical properties of the host–guest system, the photoluminescence spectra of PFO–PBD (30 wt %) films with different doping concentrations of **2** were

(16) Shi, M. Ph.D. Dissertation, Fudan University, 2005.

(17) Wu, F. I.; Su, H. J.; Shu, C. F.; Luo, L. Y.; Diao, W. G.; Cheng, C. H.; Duan, J. P.; Lee, G. H. *J. Mater. Chem.* **2005**, *15*, 1035.

(18) Thomas, K. R. J.; Velusamy, M.; Lin, J. T.; Chien, C. H.; Tao, Y. T.; Wen, Y. S.; Hu, Y. H.; Chou, P. T. *Inorg. Chem.* **2005**, *44*, 5677.

(19) Gong, X.; Lim, S. H.; Ostrowski, J. C.; Moses, D.; Bardeen, C. J.; Bazan, G. C. *J. Appl. Phys.* **2004**, *95*, 948.

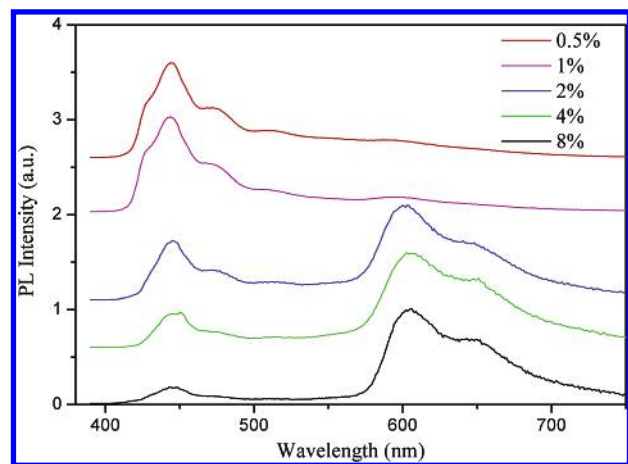


**Figure 5.** Photoluminescence spectra of 2/PFO-PBD (30 wt %) films with different doping concentrations of 2.

measured and are shown in Figure 5. It can be seen from Figure 5 that the contribution of the host emission decreases significantly with an increase in the doping concentration. When the doping concentration reaches 2 wt %, the emission of the host is weaker than that of the guest. At 8 wt % of the doping concentration, the emission of the host is almost quenched and the iridium complex emission is dominant. To further study the energy transfer of the host-guest system, the emission lifetime monitored at  $\lambda = 445$  nm (the peak emission of the host) was measured to be 0.87, 0.81, 0.66, 0.56, and 0.53 ns at doping concentrations of 0.5, 1, 2, 4, and 8 wt %, respectively (see Table S1 in the Supporting Information). With an increase in the doping concentration of the guest, the emission lifetime of the film at 445 nm becomes shorter, indicating energy transfer from the host to the guest for the opening of the fast decay channel. A higher concentration of the guest induces a shorter emission lifetime of the host and more efficient energy transfer from the host to the guest.

In addition, to investigate the self-quenching of the emission of complex 2, PMMA films with different doping concentrations of 2 were prepared and the absolute photoluminescence quantum efficiencies of these films were measured. The photoluminescence quantum efficiencies are 3.7, 7.3, 8.4, 7.2, and 6.6% at doping concentrations of 0.5, 1, 2, 4, and 8 wt %, respectively. With an increase in the doping concentration, the photoluminescence quantum efficiency of 2 increases. When the doping concentration is 2 wt %, the photoluminescence quantum efficiency reaches a maximum. When we continue to increase the doping concentration, the photoluminescence quantum efficiency decreases, which may be due to T-T annihilation and/or concentration quenching.

**Electroluminescent Devices.** Recently, polymer-based electrophosphorescent light-emitting diodes (PLEDs) have been attracting a great deal of attention, because they can be fabricated by solution processing and are suitable for large-area and flexible displays.<sup>8,20</sup> To demonstrate the basic electrophosphorescent properties, we selected complex 5 with longer wavelength (630 nm) photoluminescence and complex 2 with shorter wavelength (605 nm) photoluminescence for the fabrication of PLEDs and investigated their performances. The devices consist of the multilayer configuration ITO/PEDOT:PSS/PVK (40 nm)/PFO + PBD (30 wt %):2% iridium complex (75 nm)/Ba/Al, where

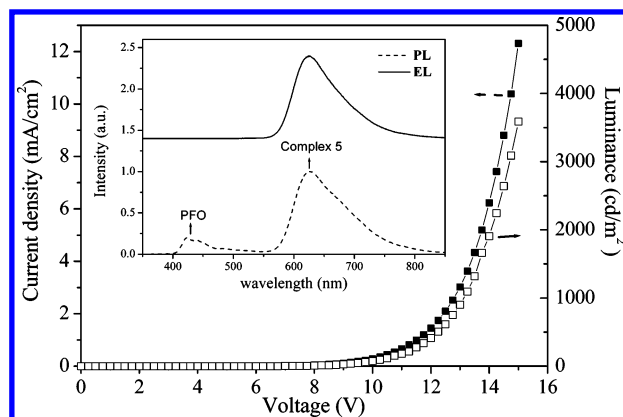


**Figure 6.**  $I$ - $V$ - $L$  characteristics for the device of 5. Inset: photoluminescent and electroluminescent spectra of a complex 5 (2 wt %)/PFO + PBD (30 wt %) film.

**Table 4. Electrophosphorescence Data for Devices Doped with Complexes 2, 5, and 7**

complex	$\eta_{\text{ext}}$ , %	$\eta_c$ , $\text{cd A}^{-1}$	voltage, V	$\lambda_{\text{max}}^{\text{EL}}$ , nm	luminance, $\text{cd m}^{-2}$	CIE ( $x$ , $y$ )
2	8.6	8.2	11.7	607	6464	0.63, 0.36
5	7.0	4.6	13.5	625	3588	0.66, 0.34
7	9.6	10.4	9.3	602	10033	0.62, 0.38

PVK is poly(vinylcarbazole). To improve hole injection and to increase substrate smoothness, a thin film of PEDOT:PSS was spin-cast onto a precleaned ITO surface and then baked at 80 °C for 12 h under vacuum. Due to its good hole-transporting properties, a layer of PVK was used as the hole-transporting layer. PFO was blended with PBD because PBD is a good electron-transporting material. The emitting layer PFO-PBD (30 wt %), doped with 2 or 5, was then spin-cast onto the surface of PVK. The conjugated polymer PFO was chosen as the host material because of its high fluorescent properties and good charge-transporting properties. Furthermore, highly efficient energy transfer can be realized because of suitable overlap between the emission spectrum of PFO-PBD and the absorption spectrum of the iridium complex.

The photoluminescent and electroluminescent spectra of the blend film 5 (2 wt %)/PFO + PBD (30 wt %) were investigated and are shown in Figure 6 (inset). The photoluminescence profile of the blend contains two components corresponding to the emission of PFO + PBD and 5, respectively. For the same doping concentration of 5, the host emission is quenched completely in the EL spectrum. The difference between PL and EL spectra indicates that both Förster energy transfer and direct charge-trapping/recombination on the iridium complex are responsible for the electroluminescence. Figure 6 shows the current density ( $I$ )-voltage ( $V$ )-luminance ( $L$ ) characteristic of the device [(ITO/PEDOT:PSS/PVK (40 nm)/PFO + PBD (30 wt %):2 wt % iridium complex (75 nm)/Ba/Al) of 5. The electroluminescence data are summarized in Table 4. For the device of 5, the maximum luminance is 3588  $\text{cd m}^{-2}$  at 13.5 V. The luminous efficiencies  $\eta_c$  and  $\eta_{\text{ext}}$  are 4.6  $\text{cd A}^{-1}$  and 7.0%, respectively. For the device of 2, the maximum luminance is 6464  $\text{cd m}^{-2}$  at 11.7 V. The luminous efficiency and external quantum efficiency are 8.2  $\text{cd A}^{-1}$  and 8.6%, respectively. The variation of ligands from biphenyl to 2-naphthyl induced significant bathochromic shifts ( $\sim 18$  nm) in the EL spectra (see Table 4). The corresponding CIE chromaticity coordinates are  $x = 0.63$ ,  $y = 0.36$  for 2 and  $x = 0.66$ ,  $y = 0.34$  for 5, respectively. The device of complex 5 shows saturated red emission.

(20) (a) Chen, X. W.; Liao, J. L.; Liang, Y. M.; Ahmed, M. O.; Tseng, H. E.; Chen, S. A. *J. Am. Chem. Soc.* **2003**, *125*, 636. (b) Gong, X.; Ostrowski, J. C.; Bazan, G. C.; Moses, D.; Heeger, A. J.; Liu, M. S.; Jen, A. K. Y. *Adv. Mater.* **2003**, *15*, 45.

In addition, to investigate the effect of different  $\beta$ -diketonate ligands on the electroluminescent properties, we also fabricated a device doped with **7**, which has the same C $\wedge$ N cyclometalated ligand and different  $\beta$ -diketonate ligands in comparison with **2**. The electroluminescent data are given in Table 4. In comparison with **2**, the device performance including  $\eta_{\text{ext}}$ ,  $\eta_{\text{c}}$ , and luminance are all improved significantly (see Table 4). This is in accordance with the improvement of photoluminescence quantum efficiency for **7**.

### Conclusion

In summary, we have identified viable operating principles for the modulation of optical properties of the iridium complexes based on different quinoline derivatives and  $\beta$ -diketonate ligands. The effects of C $\wedge$ N cyclometalated ligands and  $\beta$ -diketonate ligands on the photophysical and electrochemical properties were studied. All complexes are red emitters, and the emissive wavelength can be tuned from 596 to 634 nm. Importantly, the replacement of acac with PMIP could improve the photoluminescence quantum efficiency for this class of iridium complexes. Efficient electrophosphorescent PLEDs using **2**, **5**, and **7** as the dopants were fabricated. The device based on **2** exhibits good electroluminescent performances with a luminous efficiency of 8.2 cd A $^{-1}$ . Also, the device of **5** shows saturated red emission with CIE color coordinates of (0.66, 0.34). In addition, when acac is replaced with PMIP, the device

of complex **7** gives better performance than that of **2**. This result shows that introducing PMIP improves the device performance. More detailed studies on the fabrication and testing of devices based on other complexes are underway.

While we were finishing the synthesis and photophysical measurements of all iridium complexes in this paper, we noticed that two publications on similar Ir(III) complexes were published, which are listed as refs 17 and 18. In ref 17, Shu *et al.* reported the efficient electrophosphorescent PLED of two new iridium complexes based on the quinoline ligands and acac. In ref 18, Lin *et al.* reported the efficient electrophosphorescent OLED of a series of iridium complexes based on lepidine derivatives and acac.

**Acknowledgment.** We thank the National Natural Science Foundation of China (Nos. 20490210 and 20501006), Shanghai Science and Technology Community (No. 05DJ14004), and Huo Yingdong Education Foundation (No. 104012) for financial support.

**Supporting Information Available:** CIF files giving crystal data for **2** and **3**, figures giving excitation, phosphorescence, and UV-vis spectra, and a table giving emission lifetimes. This material is available free of charge via the Internet at <http://pubs.acs.org>.

OM060037D